
causalAssembly: Generating Realistic Production Data for Benchmarking Causal Discovery

Konstantin Göbler^{1,3} Tobias Windisch² Tim Pychynski³
Steffen Sonntag³ Martin Roth³ Mathias Drton¹

¹Technical University Munich ²University of Applied Sciences Kempten

³Robert Bosch GmbH

{konstantin.goebler, mathias.drton}@tum.de

{steffen.sonntag, tim.pychynski, martin.roth2}@de.bosch.com

tobias.windisch@hs-kempten.de

Abstract

Algorithms for causal discovery have recently undergone rapid advances and increasingly draw on flexible nonparametric methods to process complex data. With these advances comes a need for adequate empirical validation of the causal relationships learned by different algorithms. However, for most real data sources true causal relations remain unknown. This issue is further compounded by privacy concerns surrounding the release of suitable high-quality data. To help address these challenges, we gather a complex dataset comprising measurements from an assembly line in a manufacturing context. This line consists of numerous physical processes for which we are able to provide ground truth causal relationships on the basis of a detailed study of the underlying physics. We use the assembly line data and associated ground truth information to build a system for generation of semisynthetic manufacturing data that supports benchmarking of causal discovery methods. To accomplish this, we employ distributional random forests in order to flexibly estimate and represent conditional distributions that may be combined into joint distributions that strictly adhere to a causal model over the observed variables. The estimated conditionals and tools for data generation are made available in our Python library `causalAssembly`. Using the library, we showcase how to benchmark several well-known causal discovery algorithms.

1 Introduction

Causal discovery is the process of learning causal relations among variables of interest from data. In recent years, the area has seen numerous theoretical and algorithmic developments; for an overview see, e.g., [1–5]. Causal structure learning is also gaining traction in industrial domains, compare e.g. the review in [6], where knowledge about causal relations forms the basis for downstream operations such as root-cause analysis [7].

Despite the recent advances and expanded application areas, it remains challenging to provide adequate empirical validation of the causal relationships inferred by causal discovery algorithms [8, 9]. Ground truth causal relationships are unknown for most real-world examples that involve complex data sources. In addition, privacy concerns often hinder the release of high-quality data. As a result, research papers proposing novel procedures tend to evaluate structure learning performance in simplistic simulation setups that tend to have limited generalizability to real-world settings [10, 11]. When applied to real data and assessed by domain experts, results are often sobering [2, 12].

To help address these challenges, we present a complex production dataset that consists of measurements from a highly automated assembly line in a manufacturing plant. The assembly line is

composed of multiple production cells or stations (we use both terms interchangeably) along which individual components are joined together. Each individual manufacturing process highly depends on the state of the preceding processes as well as on the raw components added in earlier cells. Due to the intricate and often nonlinear nature of the physical processes—including, for example, the interaction of machine state, process control settings and component state—complex causal relationships arise across the entire assembly line. In the manufacturing plant, the individual processes are computer-monitored, and the resulting process measurements are stored throughout production.

From the assembly line, we select a subset of production cells within each of which individual processes take place for which we are able to provide ground truth causal relationships. We achieve this by carefully studying the physical processes that take place in each of the cells. In addition, in order to connect the measurements available for different processes in a flexible nonparametric manner we apply sparse additive models (SpAM) [13].

Next, we utilize the real assembly line data and associated ground truth information to construct a semisynthetic data generation tool implemented in the Python library `causalAssembly`. Synthesis is performed by estimating the conditional distributions indicated by the ground truth causal structure using distributional random forests (DRF) [14, 15]. By combining the conditionals, we create a joint distribution that strictly obeys a causal model over the observed variables.

Our contributions. We summarize our main contributions below:

- We create a highly complex assembly line dataset with associated ground truth based on which we propose a semisynthetic data generation pipeline that is implemented in the Python library `causalAssembly`. Using the library, one can easily generate data of varying dimension and complexity in order to benchmark causal discovery algorithms.
- The proposed procedure to synthesize real data is general and can in principle be applied to any given dataset with partially known domain knowledge regardless of the domain.
- We provide first benchmark results of popular causal discovery algorithms such as the PC algorithm [16], DirectLiNGAM [17], NOTEARS [18], and GraN-DAG [19].

In the remainder of this paper, we first address identifiability concerns and provide an overview of related work (Section 2). In Section 3, we describe the data generation pipeline. Section 4 demonstrates benchmarking results, and Section 5 concludes. Supplementary Sections A-C provide additional information regarding data, algorithms and metrics used, as well as additional benchmark results.

2 Identifiability and common benchmarking strategies

2.1 General background

For natural number $p \in \mathbb{N}$, let $[p] := \{1, \dots, p\}$. Defining the vertex set as $V = [p]$, let $G = (V, E)$ be a directed acyclic graph (DAG) with edge set $E \subset V \times V$. We always assume that V indexes a collection of jointly distributed random variables $(X_v)_{v \in V}$. For a subset $S \subseteq V$, we write $X_S := (X_s)_{s \in S}$ for the collection of variables indexed by S . We often write $v \rightarrow w$ or $X_v \rightarrow X_w$ instead of (v, w) to indicate the existence of an edge from v to w in G . Furthermore, a node $v \in V$ is a *parent* of another node $w \in V$ if $v \rightarrow w \in E$. The set of all parents of w in G is denoted by $pa_G(w)$. A *directed path* from v to w in G is a sequence of nodes v_1, \dots, v_k starting at $v_1 = v$ and ending at $v_k = w$ with subsequent nodes connected by edges $v_i \rightarrow v_{i+1} \in E$. Call v an *ancestor* of w if there exists a directed path from v to w , and call v a *descendant* of w if there exists a directed path from w to v . The sets of all ancestors and all descendants of node w in G are denoted $an_G(w)$ and $de_G(w)$, respectively. When it is clear which graph G is being considered, we simply write $pa(w)$, $de(w)$ or $an(g)$. A permutation $\pi : [p] \rightarrow [p]$ is a causal ordering if $\pi(v) < \pi(w)$ for all (v, w) with $w \in de_G(v)$. Such an ordering exists for every DAG, albeit not necessarily a unique one.

Throughout the remainder of this work, we assume that V is partitioned into K subsets V_1, \dots, V_K such that for all $s, t \in [K]$ with $s < t$, the nodes in V_t cannot be ancestors of nodes in V_s . A graph with such a partitioned vertex set is sometimes called a *layered digraph* [20]. Later, the partitions V_1, \dots, V_K correspond to the measurements from K sequentially performed manufacturing processes in a given assembly line. Often we have to consider all nodes up to a certain process and, thus, define

$V_{1:s} := \cup_{i=1}^{s-1} V_i$ for $s \in [K]$. Note that $V_s \cap V_{1:s} = \emptyset$. The DAG G indicates causal relationships among the random variables, and we say that X_v is a direct cause of X_w if $v \rightarrow w$. Furthermore, X_v may be an indirect cause of X_w if there is a directed path from v to w ; we refer to [21, 22] for more background. Clearly, in a layered digraph, no variable with index in V_i can be a direct or indirect cause of any node in V_s with $s < i$.

Each DAG G on V gives rise to a statistical model for the joint distribution P_X of the random vector $X = (X_v)_{v \in V}$. Here, the edges in G encode the permitted conditional dependence relations among the variables [see e.g. 23, 24]. Any distribution that satisfies the conditional independence constraints implied by G is said to be *Markov* with respect to G . In other words, the joint density of X factors into a product of conditional densities as $p(x) = \prod_{v \in V} p(x_v | x_{pa_G(v)})$ with $p(x_v | x_\emptyset) = p(x_v)$. The conditional independence relations holding in all such factorizing distributions can be obtained using the graphical criterion of *d-separation* [21]. A distribution P_X is *Markov* and *faithful* with respect to the underlying DAG G if the conditional independence relations in P_X correspond exactly to d-separation relations in G . Different DAGs may share the same set of conditional independence statements. Such DAGs are said to be Markov equivalent. All equivalent DAGs form a Markov equivalence class (MEC) [see e.g. 16].

2.2 Identifiability of the causal structure

In general, the DAG G is not identifiable from P_X alone. Learning the causal structure or its corresponding MEC from data requires assumptions. Under the Markov and faithfulness conditions regarding P_X , G can be recovered up to its MEC. Prominent routines that operate under this assumption are, for example, the PC [16] and the Greedy Equivalence Search (GES) [25] algorithm. Under additional assumptions, we may not only recover the MEC of G but G itself. Note, that the graphical model that is associated with G can also be expressed in terms of a structural equation model (SEM) [26]. That is, if P_X is Markov with respect to G then there exist independent noise variables $\epsilon = (\epsilon_1, \dots, \epsilon_p)$ and measurable function g_i such that $X_i = g_i(X_{pa(i)}, \epsilon_i)$ for all $i \in [p]$. In this framework, if all the g_i are linear and all ϵ_i follow non-Gaussian distributions—termed Linear Non-Gaussian Acyclic Model (LiNGAM)—then the causal graph is identifiable from data [27]. A comprehensive treatment of this model and various extensions is given in [28]. In a different vein, identifiability of G is also achieved under an additive noise model (ANM) [29]. In other words, as long as all g_i are non-linear as defined in [29], the noise ϵ_i may follow any distribution given that it is additive. A generalization to the post-nonlinear model is proposed by [30]. Linear SEMs with Gaussian noise terms are not identifiable. However, identifiability can be achieved in this setting under assumptions such as equal noise variances [31], where a causal order is found by sorting (conditional) variances [32].

2.3 Additive noise models for synthetic data generation

Comprehensive assessment of methods for learning causal relations is challenging due to the scarcity of real data where true causal relations are known. Hence, the focus is then often on simulated synthetic data. In order to accommodate non-linearities and also to ensure identifiability of the true DAG, ANMs are often employed for this purpose. However, synthetic data generation can leave unintended traces hinting at the true causal relations among the variables. In particular, the work of [11] demonstrates that for commonly used simulation setups involving ANMs, irrespective of the choice of the functions g_i , ordering nodes by increasing marginal variance tends to agree with the causal order of the ANM. The authors introduce *varsortability*, a score that measures the degree of concordance between causal orders of the ground truth DAG and the order of increasing marginal variance [11, Section 3.1]. When *varsortability* equals one then all directed paths lead from lower variance nodes to higher variance nodes. This is connected to the aforementioned identifiability results for linear SEMs with equal variance [32, 31]. Many of the recently proposed continuous optimization based structure learning algorithms report a similar data generative setup based on ANMs, see among others [18, 33, 19, 34–36]. The resulting high *varsortability* on the raw data scale contributes to often staggering performances of these methods as they often inadvertently make use of variance order. In real systems, on the other hand, measurement scales are essentially irrelevant for the causal order. Therefore, standardization would be a simple solution to render data scale non-informative. Yet, remnants of high *varsortability* with distinctive covariance patterns may remain even after standardization [11, 37]. Ultimately, all synthetic data generation processes are vulnerable to a lack of portraying common themes observable from practice.

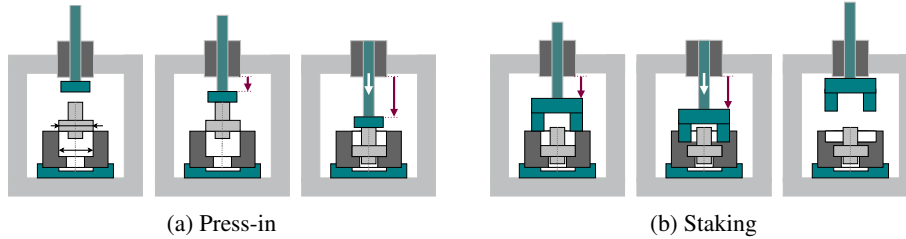


Figure 1: Illustration of the various phases of a press-in and staking process.

Evaluating the performance of algorithms is a key factor that impacts which research directions the field is gravitating towards. This can be seen, for instance, in the case of continuous optimization-based structure learning. Following the development of NOTEARS [18], numerous extensions have been proposed in short succession (see [4] for an overview). However, when evaluated outside of ANMs, performance often drops notably [12]. Therefore, there is a clear necessity for more robust evaluation techniques in the field of causal discovery as outlined in [9, 8]. This motivates the present work which seeks to support benchmarking of causal discovery by providing tools for semisynthetic data generation that draw on partial ground truth and real data from a manufacturing plant.

2.4 Related work

Focusing on observational data, the available tools for empirical illustration and benchmarking of causal discovery algorithm can be broadly classified into three tiers: (1) Real datasets with expert-knowledge driven ground truth, such as the cause-effect pairs of [38] and data pertaining to model organisms/already well understood systems in biology [39–41]. (2) Synthetic datasets generated based on well-established parameterizations [42–44]. (3) Data generated using functional specifications (see [45, 10] for recent benchmarking tools). In recent years, causal discovery benchmark challenges have also been hosted in cooperation with special conference tracks, e.g., *GSK.ai CausalBench challenge* at ICLR 2023 or *Causality 4 Climate* at NeurIPS 2019.

3 Data generation procedure

3.1 Modelling expert knowledge

Establishing partial ground truth In this work, the real-world data come from an assembly line at a manufacturing plant of Robert Bosch GmbH. We focus on a selected subset of production stations at which press-in and staking processes are executed (see Figure 2). In the following, we give a brief overview of these processes. A more in depth discussion of the relations among the central features of the physical procedures is given in supplementary Section A.1.

Press-in: In each fitting process, two components are joined in a pressing machine to form a mechanically strong and sometimes even leakage tight connection between the components. An inner cylindrical component (e.g., a valve, axle or pin) is pushed into a slightly smaller bore of a larger component. This is achieved by applying a mechanical force high enough to overcome the required friction force. After the friction force is exceeded, the inner component will move into the bore. The pressing machine stops as soon as a certain predefined press-in force is exceeded for the first time.

Staking: A staking process is an extension of a press-in process. The objective of staking is to fixate the inner component in its final position by permanently deforming some outer component materials. This is achieved by applying a large enough force to the tool to create a mechanical stress-strain state in the material resulting in permanent plastic material deformation.

Figure 1 depicts these two processes in a schematic manner. In order to control and monitor these processes in real-time, important signals are measured and analyzed by a process control unit. We extract all relevant numeric measurements for each process, and together with the mapping detailed in Section A.1 they build the foundation for our data generation scheme.

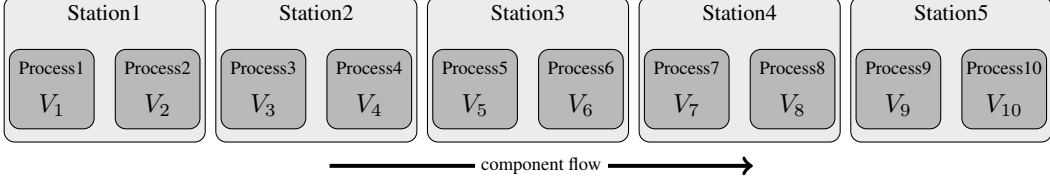


Figure 2: Illustration of the production line with five process stations each containing two successive processes. The first cell prepares components while cell two and four carry out staking tasks. The remaining cells perform press-in tasks.

3.2 Data generation in causalAssembly

Suppose the random variables $(X_v)_{v \in V}$ represent the features extracted from the manufacturing processes described above. Recall the layering introduced in Section 2.1, where we assume that $V = V_1 \dot{\cup} \dots \dot{\cup} V_K$. We extract data drawn from $K = 10$ processes carried out sequentially. These processes are lined up across five process cells such that each cell accommodates two of the production processes outlined in Figure 2. Overall we collect $|V| = 98$ features for $n = 15,581$ parts. The features distribute across production cells as follows: Station1 with $|V_1 \cup V_2| = 6$, Station2 with $|V_3 \cup V_4| = 34$, Station3 with $|V_5 \cup V_6| = 16$, Station4 with $|V_7 \cup V_8| = 26$, and Station5 with $|V_9 \cup V_{10}| = 16$.

Each individual process we chose to focus on is well understood, and we are able to state causal relations among the variables in V_s . In other words, we map the process knowledge into graphs $G_s^* = (V_s, E_s)$ for $s \in [K]$. Let $G^* := G_1^* \oplus \dots \oplus G_K^*$ be the graph union of all process graphs. Let $P_k^* := pa_{G^*}(k)$ be the set of parents for variable X_k in G^* . Note that if $k \in V_s$, then $P_k^* \subset V_s$ as well. For some measurements X_k of the s -th process, the process experts are able to state functional relations in the form $X_k \approx f_k^*(X_{P_k^*})$. However, due to their complex physical nature, our process knowledge does not extend to how the K processes may influence each other. Thus, we apply a learning step in order to find an overall causal graph $G = (V, E)$ on V , such that the induced subgraphs coincide with the expert knowledge locally, i.e., $G[V_s] = G_s^*$ for all $s \in [K]$. In this learning step we account for the known within process graph and functional structures when learning edges between the partition blocks V_1, \dots, V_K . In particular, we will not add further edges between nodes of the same process and assume that the process knowledge is ground truth. The cross-process connections will be learned from data as outlined below.

In our application, all processes are executed sequentially and process t can be influenced by all processes executed earlier. There are other assembly lines where this is not the case and where domain knowledge also contains information about inter-process influences. Such additional information could be easily inserted in our framework by imposing the restriction that the graph \mathcal{G} has no edges between V_j and V_t for the concerned indices $j < t$.

In order to infer edges across processes one could feed in $G_1^* \oplus \dots \oplus G_K^*$ as prior knowledge into causal discovery tools. However, all causal discovery algorithms impose more or less stringent assumptions regarding the data generative process. Consequently, these assumptions may carry over to our proposed semisynthetic generator, i.e., they would become features of data produced by the generator. We demonstrate this behavior in supplementary Section B.2. In an attempt to minimize this effect, we make use of sparse additive models (SpAM) [13] to learn cross-process conditional distributions, taking care to account for the (graphical) within process dependence structure as noted below. These models are flexible and non-parametric such that we minimize possible traces of the data generative procedure that might carry over to the final sampling process. We set them up such that we can easily obey the layered structure within and across cells and can build upon existing functional process knowledge.

Respecting prior knowledge in cross-process learning Let X_k be a variable from the t th process, i.e., $k \in V_t$. We want to establish which edges $j \rightarrow k$ for $j \in V_{1:t}$ ought to be included in the overall causal graph G . To this end, we consider the regression function for the residual to the functional process knowledge provided by domain experts:

$$f_k(x_{V_{1:t}}) = \mathbb{E}(X_k - f_k^*(X_{P_k^*}) \mid X_{V_{1:t}} = x_{V_{1:t}}).$$

That way, we learn the gap between process knowledge and observation using information from prior processes. If no functional process knowledge f_k^* is available for X_k , we set $f_k^* = 0$ and regress onto all variables with index in $V_{1:t} \cup P_k^*$. Sparse additive models use sums to approximate the regression function of the form $f_k(x_{V_{1:t}}) \approx \sum_{l \in V_{1:t}} f_{k,l}(x_l)$ and induce sparsity via the penalty $\sum_{l \in V_{1:t}} \|f_{k,l}\|_2$. We refer to [13, Section 2] for more details on sparse additive models. Algorithm 1 outlines our procedure to learn edges across processes.

Algorithm 1: SpAM cross-process learning

Input: Data \mathcal{D} , DAGs G_1^*, \dots, G_K^* , functions f_1^*, \dots, f_p^* , regularization parameter $\lambda \geq 0$

Output: Edge set $E_{\text{across}} \subset V \times V$.

$E_{\text{across}} \leftarrow \{\}$;

for $t = 2, \dots, K$ **do**

 Compute a causal order π_t of G_t^* ;

for k *along* π_t **do**

$S_t \leftarrow V_{1:t}$

if $f_k^* = 0$ **then**

$S_t \leftarrow S_t \cup P_k^*$

end

 Compute $(\hat{f}_{k,l})_{l \in S_t}$ with $\hat{f}_{k,l} \in \mathcal{F}_{k,l}$ that minimize:

$$\min_{f_{k,l} \in \mathcal{F}_{k,l} \text{ for } l \in S_t} \frac{1}{|\mathcal{D}|} \sum_{x \in \mathcal{D}} \left(x_k - f_k^*(x_{P_k^*}) - \sum_{l \in S_t} f_{k,l}(x_l) \right)^2 + \lambda \sum_{l \in S_t} \|f_{k,l}\|_2$$

$E_{\text{across}} \leftarrow E_{\text{across}} \cup \{(l, k) : l \in S_t, \hat{f}_{k,l} \neq 0\}$

end

end

Note that depending on the function classes $\mathcal{F}_{k,l}$, the minimization problem in Algorithm 1 becomes a convex program. Indeed, in practice, we express each X_k as a projection on to a set of cubic spline basis functions to ensure convexity. The tuning parameter $\lambda \geq 0$ is selected via cross-validation.

Algorithm 1 admits a natural way to also incorporate higher-level process knowledge. One such example would be that influences between measurements of process j and t with $j < t$ can be excluded. If such domain information is encoded as a graph \mathcal{G} on $[K]$ as described above, we set $S_t = \cup_{j \in \text{pa}_{\mathcal{G}}(t)} V_j$ instead of $S_t = V_{1:t}$.

Applying Algorithm 1 to the given process knowledge graphs, we obtain the final ground truth DAG $G_{\text{partial}}^* := (V, E \cup E_{\text{across}})$. Figure 3 illustrates G_{partial}^* .

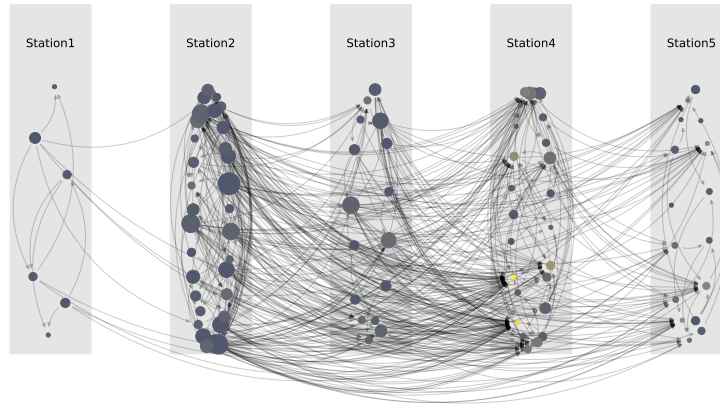


Figure 3: Assembly line ground truth after edges have been learned between processes using the SpAM procedure. Note that only the stations are shown, not the processes they are decomposed in. Node size increases with the number of out-edges. Node color gets brighter with the number of in-edges.

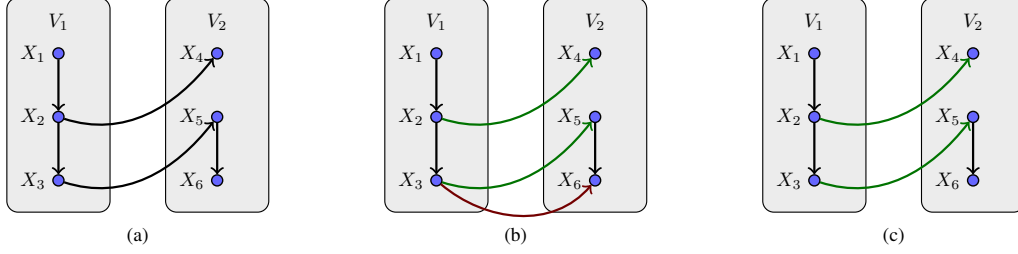


Figure 4: SpAM search illustration. Figure (a) represents the ground truth. Two scenarios are considered: In (b) naive search is performed, without taking into account the causal order of the DAG in the second station. In (c) the parental relations in Station 2 are used, resulting in the correct DAG.

Example: Consider an assembly line with two processes and decomposition $V = V_1 \cup V_2$, where we want to learn connections between V_1 and V_2 , each of which comprises three measured variables (see Figure 4). Ignoring already known parental relations for X_6 in the second process will lead to inferring incorrect edges when running the regression with predictors from the first process only, i.e., with predictor set $S_6^{\text{naive}} = \{1, 2, 3\}$; see Figure 4(b). This is true unless both processes are in fact unconnected or the second process graph is empty. Including the parent set of X_6 in G_2^* in the predictor set $S_6 = \{1, 2, 3, 5\}$ leads to correct inference of the edges across processes; see Figure 4(c).

Synthetization In order to ensure that the data used in benchmarking really come from a distribution that factorizes according to the ground truth DAG G_{partial}^* , we explicitly estimate the conditional distributions under the factorization implied by the independence constraints in G_{partial}^* . To that end, we employ distributional random forests (DRFs) [14] to obtain estimates $\hat{P}_X^{\text{DRF}}(X_k | X_{pa_{G^*}^{\text{partial}}}(k))$, $k \in V$, along a causal order of G_{partial}^* . This has been first proposed by [15] in the context of the data from [41]. Section B.1 details how DRFs are built, what splitting criterion is used, and how to estimate conditional distributions. Given $\hat{P}_X^{\text{DRF}}(X_k | X_{pa_{G^*}^{\text{partial}}}(k))$ we sample a new dataset $\mathcal{D}_{\text{synth}} \subset \mathbb{R}^p$ from the production line as outlined in Algorithm 2. By construction, $\mathcal{D}_{\text{synth}}$ is drawn from the estimated joint distribution \hat{P}_X^{DRF} and is guaranteed to be Markov with respect to the DAG G_{partial}^* .

In order to provide an option to consider data of different dimensionality, we also offer the option to focus on each one of the five process cells that constitute the natural subunits of the assembly line. Simply considering the marginal distribution of the variables in one such cell generally induces confounding (through effects of earlier cells). Hence, to allow sampling from a distribution Markov to the ground truth within-cell DAG G_s^* for cell s , we refit the DRFs and apply Algorithm 2 to each cell individually to generate data the desired within-cell dependence structure.

Algorithm 2: Sampling from the causal DRFs

Input: Finite dataset $\mathcal{D}_{\text{original}} \subset \mathbb{R}^p$, DAG G with p nodes, number of samples n to be generated

Output: A dataset $\mathcal{D}_{\text{synth}} \subset \mathbb{R}^p$ of size n

$\mathcal{D}_{\text{synth}} \leftarrow \emptyset$;

Compute a causal order π of G ;

while $|\mathcal{D}_{\text{synth}}| < n$ **do**

for k along π **do**

if $pa_G(k) = \emptyset$ **then**

 sample $\hat{x}_k \in \mathbb{R}$ via smooth bootstrapping from $\{x_k \in \mathbb{R} : x \in \mathcal{D}_{\text{original}}\}$;

else

 sample $\hat{x}_k \in \mathbb{R}$ from $\hat{P}_X^{\text{DRF}}(X_k | X_{pa_G(k)} = \hat{x}_{pa_G(k)})$;

end

$\mathcal{D}_{\text{synth}} \leftarrow \mathcal{D}_{\text{synth}} \cup \{\hat{x}\}$;

end

end

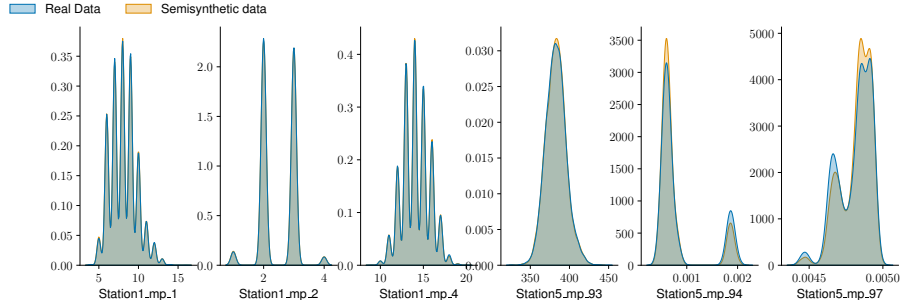


Figure 5: Kernel density plots comparing the highest (first three) and lowest (last three) agreement in terms of Kolmogorov-Smirnov statistic.

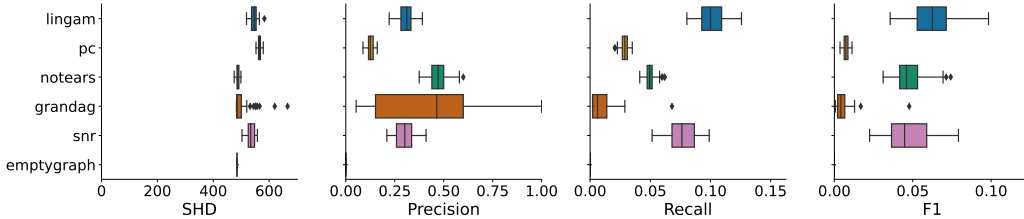


Figure 6: Chosen metrics for assessing causal discovery of the full assembly line ($|V| = 98$) using 100 simulation runs on a sample size of $n = 500$

3.3 Semisynthetic data description

To demonstrate that the semisynthetic “Markovian” data obtained from our data generation pipeline preserves key characteristics of the real data, we calculated the two-sample Kolmogorov-Smirnov statistic [46] between all variables in the real and a semisynthetic dataset. Figure 5 shows kernel density estimates of the variables with largest and smallest Kolmogorov-Smirnov statistics among all non-source nodes. Even in unfavorable cases where the absolute difference between the marginal distributions is largest, the semisynthetic data only shows moderate deviations from the real data.

4 Benchmark results

As a proof of concept, we present first causal discovery benchmark results based on data obtained from the semisynthetic data generative procedure in the `causalAssembly` library. In order to make sure that privacy concerns are respected, we proceed as follows: First, we apply the procedure to the real data from the manufacturing plant. Based on the fitted DRF we sample new data that matches the dimension of the original real data. Based on this first-level semisynthetic dataset, we conduct the benchmark study below, which establishes results for the full assembly line using the ground truth depicted in Figure 3. Additionally, we present further benchmark results based on the individual process cells in Section C.2.

The purpose of the study we report on here is simply to demonstrate the versatility of the data generation scheme. A more elaborate set of experiments comprising more causal discovery routines, varying sample size and adjusting hyperparameters will be taken up in future work.

Figure 6 reports evaluation results based on causal discovery algorithms and metrics that we described explicitly in Section C.1. In this evaluation, the data is always standardized before structure learning, and we perform 100 simulation runs. The `sortnregress` (`snr`) routine serves as a reference point, as for standardized data it corresponds to choosing some order at random and regressing (*random regress*) each node on its ancestors (see also [11]). Considering first the structural Hamming distance (SHD) to the ground truth, the studied default methods fail to beat outputting an empty graph. The fact that NOTEARS does better than the other methods here can be attributed to outputting very sparse graphs. Linear methods such as DirectLINGAM and PC algorithm with standard partial correlation

tests are on par with random regress. For GraN-DAG some higher variability in results is observed. For Precision, Recall, and F1 score, the PC algorithm fares surprisingly well. GraN-DAG shows better Recall and F1 score, but a highly variable Precision. We emphasize that these results are based on off-the-shelf implementations with no attempts to tune the methods to the nature of the data. Moreover, the considered methods also all ignore the prior knowledge provided by the layering across processes.

Although very limited, this first prototype of a benchmark study reveals that the data one may create with `causalAssembly` are challenging for standard off-the-shelf methods. This largely confirms results conducted on empirical data in the sense that learning accuracy presented in the literature on the basis of synthetic data overestimates performance on more complex datasets [12, 47].

5 Conclusion and Limitations

Empirical validation is key in understanding how causal discovery algorithms perform outside their laboratory settings. In this work, we introduce a complex dataset comprising measurements from a highly automated assembly line in a manufacturing plant, for which we are able to put together partial ground truth causal relationships on the basis of a detailed study of the underlying physics. Based on this dataset, we use the associated ground truth and develop a versatile synthetization pipeline based on distributional random forests that helps overcome common real world data problems such as lack of ground truth, confounding, and privacy concerns. The resulting data generator is implemented in the Python library `causalAssembly` and can be used to benchmark causal discovery algorithms based on complex data. We demonstrate this by providing initial benchmarking results for some well-known causal discovery algorithms.

An important limitation is that at the moment `causalAssembly` supports the generation of continuous data only. This is because features extracted from staking and press-in processes are continuous. However, the pipeline presented is more general and supports the incorporation of mixed data. We plan to include discrete features by selecting a wider range of processes in future releases of `causalAssembly`. Furthermore, the fitted conditional distributions require substantial memory, and we plan to optimize the data architecture in future releases. In addition, it would be interesting to take advantages of opportunities to involve interventional samples.

Ethical aspects and societal consequences The authors do not foresee negative societal consequences of this work.

Acknowledgments and Disclosure of Funding

We would like to thank Jens Ackermann for helpful comments and support.

The research for this project was partly conducted by authors employed at Robert Bosch GmbH. Furthermore, this project has received funding from the European Research Council (ERC) under the European Union’s Horizon 2020 research and innovation programme (grant agreement No 883818).

References

- [1] Clark Glymour, Kun Zhang, and Peter Spirtes. Review of causal discovery methods based on graphical models. *Frontiers in Genetics*, 10, June 2019. doi: 10.3389/fgene.2019.00524. URL <https://doi.org/10.3389/fgene.2019.00524>.
- [2] Christina Heinze-Deml, Marloes H. Maathuis, and Nicolai Meinshausen. Causal structure learning. *Annual Review of Statistics and Its Application*, 5(1):371–391, 2018. doi: 10.1146/annurev-statistics-031017-100630. URL <https://doi.org/10.1146/annurev-statistics-031017-100630>.
- [3] Marloes Maathuis, Mathias Drton, Steffen Lauritzen, and Martin Wainwright, editors. *Handbook of graphical models*. Chapman & Hall/CRC Handbooks of Modern Statistical Methods. CRC Press, Boca Raton, FL, 2019. ISBN 978-1-4987-8862-5.
- [4] Matthew J. Vowels, Necati Cihan Camgoz, and Richard Bowden. D’ya like DAGs? A survey on structure learning and causal discovery. *ACM Computing Surveys*, 55(4):1–36, 2022. doi: 10.1145/3527154. URL <https://doi.org/10.1145/3527154>.
- [5] Alessio Zanga, Elif Ozkirimli, and Fabio Stella. A survey on causal discovery: Theory and practice. *International Journal of Approximate Reasoning*, 151:101–129, 2022. ISSN 0888-613X. doi: <https://doi.org/10.1016/j.ijar.2022.09.004>. URL <https://www.sciencedirect.com/science/article/pii/S0888613X22001402>.
- [6] Matej Vuković and Stefan Thalmann. Causal discovery in manufacturing: A structured literature review. *Journal of Manufacturing and Materials Processing*, 6(1), 2022. ISSN 2504-4494. doi: 10.3390/jmmp6010010. URL <https://www.mdpi.com/2504-4494/6/1/10>.
- [7] Kailash Budhathoki, Lenon Minorics, Patrick Bloebaum, and Dominik Janzing. Causal structure-based root cause analysis of outliers. In *Proceedings of the 39th International Conference on Machine Learning*, volume 162 of *Proceedings of Machine Learning Research*, pages 2357–2369. PMLR, 17–23 Jul 2022. URL <https://proceedings.mlr.press/v162/budhathoki22a.html>.
- [8] Amanda Gentzel, Dan Garant, and David Jensen. The case for evaluating causal models using interventional measures and empirical data. In *Advances in Neural Information Processing Systems*, volume 32. Curran Associates, Inc., 2019. URL https://proceedings.neurips.cc/paper_files/paper/2019/file/a87c11b9100c608b7f8e98cfa316ff7b-Paper.pdf.
- [9] Marco Eigenmann, Sach Mukherjee, and Marloes Maathuis. Evaluation of causal structure learning algorithms via risk estimation. In *Proceedings of the 36th Conference on Uncertainty in Artificial Intelligence (UAI)*, volume 124 of *Proceedings of Machine Learning Research*, pages 151–160. PMLR, 2020. URL <https://proceedings.mlr.press/v124/eigenmann20a.html>.
- [10] Johannes Huegle, Christopher Hagedorn, Lukas Boehme, Mats Poerschke, Jonas Umland, and Rainer Schlosser. Manm-cs: Data generation for benchmarking causal structure learning from mixed discrete-continuous and nonlinear data. In *WHY-21 @ NeurIPS 2021*, 2021.
- [11] Alexander G. Reisach, Christof Seiler, and Sebastian Weichwald. Beware of the simulated DAG! Causal discovery benchmarks may be easy to game. In *Advances in Neural Information Processing Systems 34 (NeurIPS)*, pages 1–13. NeurIPS Proceedings, 2021.
- [12] Anthony C. Constantinou, Yang Liu, Kiattikun Chobtham, Zhigao Guo, and Neville K. Kitson. Large-scale empirical validation of Bayesian network structure learning algorithms with noisy data. *International Journal of Approximate Reasoning*, 131:151–188, 2021. doi: 10.1016/j.ijar.2021.01.001. URL <https://doi.org/10.1016/j.ijar.2021.01.001>.
- [13] Pradeep Ravikumar, John Lafferty, Han Liu, and Larry Wasserman. Sparse additive models. *J. R. Stat. Soc. Ser. B Stat. Methodol.*, 71(5):1009–1030, 2009. ISSN 1369-7412,1467-9868. doi: 10.1111/j.1467-9868.2009.00718.x. URL <https://doi.org/10.1111/j.1467-9868.2009.00718.x>.

- [14] Domagoj Cevid, Loris Michel, Jeffrey Näf, Peter Bühlmann, and Nicolai Meinshausen. Distributional random forests: Heterogeneity adjustment and multivariate distributional regression. *Journal of Machine Learning Research*, 23(333):1–79, 2022. URL <http://jmlr.org/papers/v23/21-0585.html>.
- [15] Juan L. Gamella, Armeen Taeb, Christina Heinze-Deml, and Peter Bühlmann. Characterization and greedy learning of Gaussian structural causal models under unknown interventions. *arXiv preprint arXiv:2211.14897*, 2022.
- [16] Peter Spirtes, Clark Glymour, and Richard Scheines. *Causation, prediction, and search*, volume 81 of *Lecture Notes in Statistics*. Springer-Verlag, New York, 1993. ISBN 0-387-97979-4. doi: 10.1007/978-1-4612-2748-9. URL <https://doi.org/10.1007/978-1-4612-2748-9>.
- [17] Shohei Shimizu, Takanori Inazumi, Yasuhiro Sogawa, Aapo Hyvärinen, Yoshinobu Kawahara, Takashi Washio, Patrik O. Hoyer, and Kenneth Bollen. DirectLiNGAM: A direct method for learning a linear non-Gaussian structural equation model. *Journal of Machine Learning Research*, 12(33):1225–1248, 2011. URL <http://jmlr.org/papers/v12/shimizu11a.html>.
- [18] Xun Zheng, Bryon Aragam, Pradeep K Ravikumar, and Eric P Xing. Dags with no tears: Continuous optimization for structure learning. In *Advances in Neural Information Processing Systems*, volume 31. Curran Associates, Inc., 2018. URL https://proceedings.neurips.cc/paper_files/paper/2018/file/e347c51419ffb23ca3fd5050202f9c3d-Paper.pdf.
- [19] Sébastien Lachapelle, Philippe Brouillard, Tristan Deleu, and Simon Lacoste-Julien. Gradient-based neural DAG learning. In *International Conference on Learning Representations*, 2020. URL <https://openreview.net/forum?id=rklbKA4YDS>.
- [20] Patrick Healy and Nikola S. Nikolov. A branch-and-cut approach to the directed acyclic graph layering problem. In *Graph drawing*, volume 2528 of *Lecture Notes in Comput. Sci.*, pages 98–109. Springer, Berlin, 2002. ISBN 3-540-00158-1. doi: 10.1007/3-540-36151-0_{_}10. URL https://doi.org/10.1007/3-540-36151-0_10.
- [21] Judea Pearl. *Causality*. Cambridge University Press, Cambridge, second edition, 2009. ISBN 978-0-521-89560-6; 0-521-77362-8. doi: 10.1017/CBO9780511803161. URL <https://doi.org/10.1017/CBO9780511803161>. Models, reasoning, and inference.
- [22] Jonas Peters, Dominik Janzing, and Bernhard Schölkopf. *Elements of causal inference: Foundations and learning algorithms*. Adaptive Computation and Machine Learning. MIT Press, Cambridge, MA, 2017. ISBN 978-0-262-03731-0. URL <https://mitpress.mit.edu/books/elements-causal-inference>.
- [23] Mathias Drton and Marloes H. Maathuis. Structure learning in graphical modeling. *Annual Review of Statistics and Its Application*, 4(1):365–393, 2017. doi: 10.1146/annurev-statistics-060116-053803. URL <https://doi.org/10.1146/annurev-statistics-060116-053803>.
- [24] Steffen L. Lauritzen. *Graphical models*, volume 17 of *Oxford Statistical Science Series*. The Clarendon Press, Oxford University Press, New York, 1996. ISBN 0-19-852219-3. Oxford Science Publications.
- [25] David Maxwell Chickering. Optimal structure identification with greedy search. *J. Mach. Learn. Res.*, 3:507–554, 2003. ISSN 1532-4435. doi: 10.1162/153244303321897717. URL <https://doi.org/10.1162/153244303321897717>.
- [26] Kenneth A. Bollen. *Structural equations with latent variables*. Wiley Series in Probability and Mathematical Statistics: Applied Probability and Statistics. John Wiley & Sons, Inc., New York, 1989. ISBN 0-471-01171-1. doi: 10.1002/9781118619179. URL <https://doi.org/10.1002/9781118619179>. A Wiley-Interscience Publication.
- [27] Shohei Shimizu, Patrik O. Hoyer, Aapo Hyvärinen, and Antti Kerminen. A linear non-Gaussian acyclic model for causal discovery. *J. Mach. Learn. Res.*, 7:2003–2030, 2006. ISSN 1532-4435,1533-7928.

- [28] Shohei. Shimizu. *Statistical causal discovery: LiNGAM approach*. JSS Research Series in Statistics. Springer Japan, Tokyo, 1st ed. 2022. edition, 2022. ISBN 9784431557845.
- [29] Patrik Hoyer, Dominik Janzing, Joris M Mooij, Jonas Peters, and Bernhard Schölkopf. Nonlinear causal discovery with additive noise models. In *Advances in Neural Information Processing Systems*, volume 21. Curran Associates, Inc., 2008. URL https://proceedings.neurips.cc/paper_files/paper/2008/file/f7664060cc52bc6f3d620bcdec94a4b6-Paper.pdf.
- [30] Kun Zhang and Aapo Hyvärinen. On the identifiability of the post-nonlinear causal model. In *Proceedings of the Twenty-Fifth Conference on Uncertainty in Artificial Intelligence, UAI '09*, pages 647–655, Arlington, Virginia, USA, 2009. AUAI Press. ISBN 9780974903958.
- [31] J. Peters and P. Bühlmann. Identifiability of Gaussian structural equation models with equal error variances. *Biometrika*, 101(1):219–228, 2014. ISSN 0006-3444,1464-3510. doi: 10.1093/biomet/ast043. URL <https://doi.org/10.1093/biomet/ast043>.
- [32] Wenyu Chen, Mathias Drton, and Y. Samuel Wang. On causal discovery with an equal-variance assumption. *Biometrika*, 106(4):973–980, 2019. ISSN 0006-3444. doi: 10.1093/biomet/asz049. URL <https://doi-org.eaccess.tum.edu/10.1093/biomet/asz049>.
- [33] Ignavier Ng, AmirEmad Ghassami, and Kun Zhang. On the role of sparsity and DAG constraints for learning linear DAGs. In *Advances in Neural Information Processing Systems*, volume 33, pages 17943–17954. Curran Associates, Inc., 2020. URL https://proceedings.neurips.cc/paper_files/paper/2020/file/d04d42cdf14579cd294e5079e0745411-Paper.pdf.
- [34] Yue Yu, Tian Gao, Naiyu Yin, and Qiang Ji. DAGs with no curl: An efficient DAG structure learning approach. In *Proceedings of the 38th International Conference on Machine Learning*, volume 139 of *Proceedings of Machine Learning Research*, pages 12156–12166. PMLR, 2021. URL <https://proceedings.mlr.press/v139/yy21a.html>.
- [35] Zhen Zhang, Ignavier Ng, Dong Gong, Yuhang Liu, Ehsan M Abbasnejad, Mingming Gong, Kun Zhang, and Javen Qinfeng Shi. Truncated matrix power iteration for differentiable DAG learning. In *Advances in Neural Information Processing Systems*, 2022. URL <https://openreview.net/forum?id=I4aSjFR7j0m>.
- [36] An Zhang, Fangfu Liu, Wenchang Ma, Zhibo Cai, Xiang Wang, and Tat-Seng Chua. Boosting causal discovery via adaptive sample reweighting. In *The Eleventh International Conference on Learning Representations*, 2023. URL <https://openreview.net/forum?id=LNpMtk15AS4>.
- [37] Alexander G. Reisach, Myriam Tami, Christof Seiler, Antoine Chambaz, and Sebastian Weichwald. Simple sorting criteria help find the causal order in additive noise models. *arXiv preprint arXiv:2303.18211*, 2023.
- [38] Joris M. Mooij, Jonas Peters, Dominik Janzing, Jakob Zscheischler, and Bernhard Schölkopf. Distinguishing cause from effect using observational data: Methods and benchmarks. *Journal of Machine Learning Research*, 17(32):1–102, 2016. URL <http://jmlr.org/papers/v17/14-518.html>.
- [39] Daniel Marbach, James C Costello, Robert Küffner, Nicole M Vega, Robert J Prill, Diogo M Camacho, Kyle R Allison, Manolis Kellis, James J Collins, and Gustavo Stolovitzky. Wisdom of crowds for robust gene network inference. *Nature Methods*, 9(8):796–804, 2012. doi: 10.1038/nmeth.2016. URL <https://doi.org/10.1038/nmeth.2016>.
- [40] Joseph M. Replogle, Reuben A. Saunders, Angela N. Pogson, Jeffrey A. Hussmann, Alexander Lenail, Alina Guna, Lauren Mascibroda, Eric J. Wagner, Karen Adelman, Gila Lithwick-Yanai, Nika Iremadze, Florian Oberstrass, Doron Lipson, Jessica L. Bonnar, Marco Jost, Thomas M. Norman, and Jonathan S. Weissman. Mapping information-rich genotype-phenotype landscapes with genome-scale perturb-seq. *Cell*, 185(14):2559–2575.e28, 2022. doi: 10.1016/j.cell.2022.05.013. URL <https://doi.org/10.1016/j.cell.2022.05.013>.

- [41] Karen Sachs, Omar Perez, Dana Pe'er, Douglas A. Lauffenburger, and Garry P. Nolan. Causal protein-signaling networks derived from multiparameter single-cell data. *Science*, 308(5721): 523–529, 2005. doi: 10.1126/science.1105809. URL <https://www.science.org/doi/abs/10.1126/science.1105809>.
- [42] Tim Van den Bulcke, Koenraad Van Leemput, Bart Naudts, Piet van Remortel, Hongwu Ma, Alain Verschoren, Bart De Moor, and Kathleen Marchal. SynTREN: A generator of synthetic gene expression data for design and analysis of structure learning algorithms. *BMC Bioinformatics*, 7(1), 2006. doi: 10.1186/1471-2105-7-43. URL <https://doi.org/10.1186/1471-2105-7-43>.
- [43] Thomas Schaffter, Daniel Marbach, and Dario Floreano. GeneNetWeaver: In silico benchmark generation and performance profiling of network inference methods. *Bioinformatics*, 27(16): 2263–2270, 2011. ISSN 1367-4803. doi: 10.1093/bioinformatics/btr373. URL <https://doi.org/10.1093/bioinformatics/btr373>.
- [44] M. Scutari. Learning Bayesian networks with the bnlearn R package. *Journal of Statistical Software*, 35(3):1–22, 2010. URL <http://www.jstatsoft.org/v35/i03/>.
- [45] Jarry Chen and Haytham M. Fayek. The structurally complex with additive parent causality (scary) dataset. In *2nd Conference on Causal Learning and Reasoning*, 2023.
- [46] A. N Kolmogorov. Sulla determinazione empirica di una legge di distribuzione. *Giornale dell'Istituto Italiano degli Attuari*, 4:83–91, 1933. URL <https://cir.nii.ac.jp/crid/1571135650766370304>.
- [47] Felix L. Rios, Giusi Moffa, and Jack Kuipers. Benchpress: A scalable and versatile workflow for benchmarking structure learning algorithms. *arXiv preprint arXiv:2107.03863*, 2022.
- [48] Leo Breiman. Random forests. *Machine Learning*, 45(1):5–32, 2001. doi: 10.1023/a:1010933404324. URL <https://doi.org/10.1023/a:1010933404324>.
- [49] Arthur Gretton, Karsten Borgwardt, Malte Rasch, Bernhard Schölkopf, and Alex Smola. A kernel method for the two-sample-problem. In *Advances in Neural Information Processing Systems*, volume 19. MIT Press, 2006. URL https://proceedings.neurips.cc/paper_files/paper/2006/file/e9fb2eda3d9c55a0d89c98d6c54b5b3e-Paper.pdf.
- [50] Arthur Gretton, Dino Sejdinovic, Heiko Strathmann, Sivaraman Balakrishnan, Massimiliano Pontil, Kenji Fukumizu, and Bharath K. Sriperumbudur. Optimal kernel choice for large-scale two-sample tests. In *Advances in Neural Information Processing Systems*, volume 25. Curran Associates, Inc., 2012. URL https://proceedings.neurips.cc/paper_files/paper/2012/file/dbe272bab69f8e13f14b405e038deb64-Paper.pdf.
- [51] Diego Colombo and Marloes H. Maathuis. Order-independent constraint-based causal structure learning. *J. Mach. Learn. Res.*, 15:3741–3782, 2014. ISSN 1532-4435,1533-7928.
- [52] Aapo Hyvärinen and Stephen M. Smith. Pairwise likelihood ratios for estimation of non-Gaussian structural equation models. *J. Mach. Learn. Res.*, 14:111–152, 2013. ISSN 1532-4435,1533-7928.
- [53] Xun Zheng, Chen Dan, Bryon Aragam, Pradeep Ravikumar, and Eric Xing. Learning sparse non-parametric DAGs. In *Proceedings of the Twenty Third International Conference on Artificial Intelligence and Statistics*, volume 108 of *Proceedings of Machine Learning Research*, pages 3414–3425. PMLR, 2020. URL <https://proceedings.mlr.press/v108/zheng20a.html>.

Table 1: Description of relevant force and position features extracted from the measurements during the press-in process.

Parameter	Description
F_{offs}	Average force measured during closing of the gap between tool and work piece. This depends on the acceleration and mass of the tool as well as the force sensor measurement error.
F_1	Press-in force (friction force) required to reach the block position (S_1) as extracted from gradient detection algorithm.
F_2	Maximum force at the end of the process. This force depends on the structural stiffness and the difference between the positions S_2 and S_1 .
S_0	Axial position of tool at first force increase as extracted from gradient detection algorithm. Position depends on geometrical tolerances of the machine and components as well as on the calibration of the position sensor.
S_1	Axial position of tool at reaching the block position. Position depends on the relative displacement S_0 . S_1 is affected by the length of the bore as well as by the elastic deformation of the machine. Deformation is influenced by the required press-in force F_1 and by the structural machine and component stiffness. Once this gradient position is detected by the process control unit during process execution the command for reversing the tool movement is given.
S_2	Maximum tool position where the tool direction of movement is effectively reversed. This is affected by the position S_1 , by the time required for computation of the gradient point, the tool speed, by the inertial mass of the tool and by the effective structural stiffness.

Appendix

A Assembly line dataset

We introduce a complex production dataset comprising real measurements from a highly automated assembly line in a manufacturing plant. The assembly line consists of multiple production cells or stations along which individual components are joined together. Parts are processed in production stations or cells and are sequentially passed to the next according to the line structure.

Often, one production cell performs the same process several times either in succession or in parallel to reduce overall cycle time. Raw components are added to the assembly at the respective stations. The quality of the assembly process depends on the respective machine state and settings (e.g. tool state, control parameters), the environmental conditions, and on the raw state of the components or intermediates. We carefully study the physical processes that take place in each of the cells.

A.1 Mapping process knowledge

Press-in In order for the inner cylindrical component to be pressed into the bore, mechanical force has to exceed friction force. The friction force depends on component properties, such as the geometrical dimensions (especially diameters and axial lengths), structural stiffness as well as the surface conditions (e.g. surface roughness). Also, machine properties such as misalignment of the pressing machine tool with respect to the work piece holder and cylindrical bore axis can affect the process. None of these properties is measured directly for each component. Depending on the product type, the nominal values of the component properties may differ.

During the fitting process the force acting on the pressing machine tool and its current vertical position are measured jointly using special sensors. In order to control and monitor the process both signals are analyzed during and after the process by the process control unit, for example using gradient detection algorithms. The change in measured position is the sum of both the elastic deformation of the pressing machine (driven by the force and structural machine stiffness) and the actual movement of the inner component relative to the bore. Figure 7 demonstrates how the machine tool force

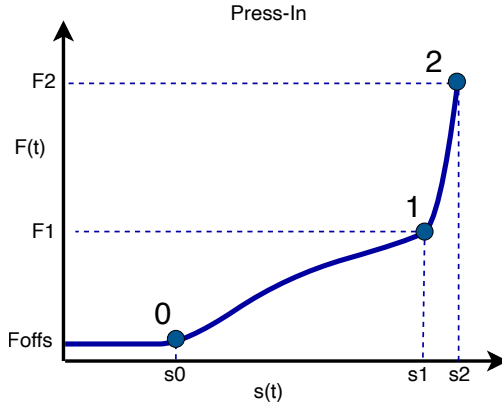


Figure 7: A typical Force (y-axis) and Position (x-axis) curve during press-in illustrating the characteristics of the process.

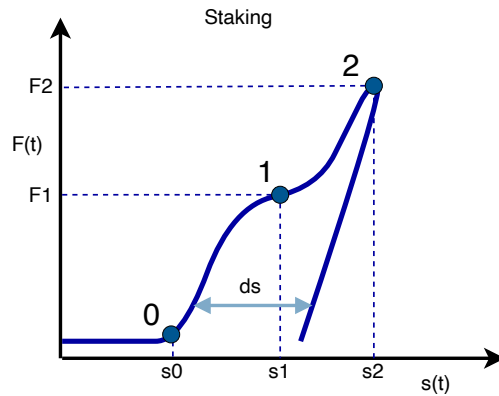


Figure 8: A typical Force (y-axis) and Position (x-axis) curve during staking illustrating the characteristics of the process.

behaves along the vertical position. The most important features extracted from this procedure are stored in the manufacturing execution system.

Staking In staking the deformation process of the material is mainly driven by two factors. One factor is the material yield strength and hardening behavior. The other factor is the compression stress. The latter is imposed by the force acting on the tool and by the contact area between tool and component. If several staking processes are happening on the same component with several bore positions, the unknown material state is likely to be similar, confounding the observed force values.

Often, press-in and staking processes are run on the same machine. Unobserved machine properties such as structural stiffness, tool misalignment and force sensor positions may impact both processes. Furthermore, confounding can be caused by similarities of the component properties (same component with several bores) or due to batch effects.

B Semisynthetic data generator

The semisynthetic data generation tool is made available through the Python library `causalAssembly` available at <https://github.com/boschresearch/causalAssembly>. We also provide the semisynthetic data itself (and for convenience one set of datasets with sample size $n = 500$) as well as the partial ground truth. All benchmark results presented both in the main text and the supplementary sections are also accessible through `causalAssembly`.

Table 2: Description of relevant force and position features extracted from the measurements during the staking process.

Parameter	Description
F_1^*	Staking force required to reach the turning point of increasing structural stiffness as extracted from the detection algorithm. Once this turning point is detected by the process control unit during process execution the process command for reversing the tool movement is given after an additional, pre-defined force delta has been exceeded.
F_2^*	Maximum force at the end of the process. This force depends on the structural stiffness and the difference between the positions S_2^* and S_1^* .
S_0^*	Axial position of tool at first force increase as extracted from gradient detection algorithm. Position depends on geometrical tolerances of the machine and components as well as on the calibration of the position sensor.
S_1^*	Axial position of tool at reaching the turning point. Position depends on the relative displacement S_0 . S_0 is affected by the length of the bore as well as by the elastic deformation of the machine. Deformation is influenced by the required press-in force F_1^* and by the structural machine and component stiffness.
S_2^*	Maximum tool position where the tool direction of movement is effectively reversed. This is affected by the position S_1^* , by the time required for computation of the turning point, the tool speed, by the inertial mass of the tool and by the effective structural stiffness.
ΔS^*	Difference in axial position of the tool after removing the pressing force measured at a pre-defined remaining force value. This indicates the true deformation length in the bore without the elastic machine deformation.

B.1 Distributional random forests

We make use of distributional random forests [14] in order to estimate conditional distributions. The procedure builds on random forests [48] where the original splitting criterion is replaced with a distributional metric in order to ensure homogeneity in each of the tree’s leaf nodes. To that end, the authors use the maximal mean discrepancy (MMD) statistic [49]. The resulting leaf nodes in the forest give rise to neighborhoods of relevant training data points. Just as in the standard random forest this induces weighting functions for each tree that quantify importance of the given training data points. The average of the tree-specific weighting functions can then be used to estimate the conditional distribution given some test data points.

In our case the conditional distribution of X_k in graph G is given by $P(X_k | X_{pa_G(k)} = x)$ for all $k \in V$. Assume we have grown N trees $\mathcal{T}_1, \dots, \mathcal{T}_N$ and denote $\mathcal{L}_j(x)$ the set of training data points that are assigned to the same leaf node as the test data point x in tree \mathcal{T}_j . [14] define the weighting function by the average of the tree-specific weighting functions i.e. $w_x(x_i) = 1/N \sum_{j=1}^N \mathbb{1}(x_i \in \mathcal{L}_j(x)) / |\mathcal{L}_j(x)|$. Estimating the conditional distribution $P(X_k | X_{pa_G(k)} = x)$ boils down to assigning weights to the point mass $\delta_{x_{ik}}$ at x_{ik} in the empirical distribution of X_k , i.e.

$$\hat{P}(X_k | X_{pa_G(k)} = x) = \sum_{i=1}^n w_x(x_i) \cdot \delta_{x_{ik}},$$

where n is the sample size of the training data.

As recommended in [14] for each conditional distribution we grow $N = 2000$ trees and choose the Gaussian kernel for the MMD splitting criterion with bandwidth chosen according to the *median heuristic* [50]. Table 4 gives an overview over the remaining hyperparameters.

B.2 Influence of initial learning

As indicated in the main text, learning edges across processes using causal discovery algorithms leaves distinct traces. Benchmarking outcomes are then tilted in favor of the routine employed in this

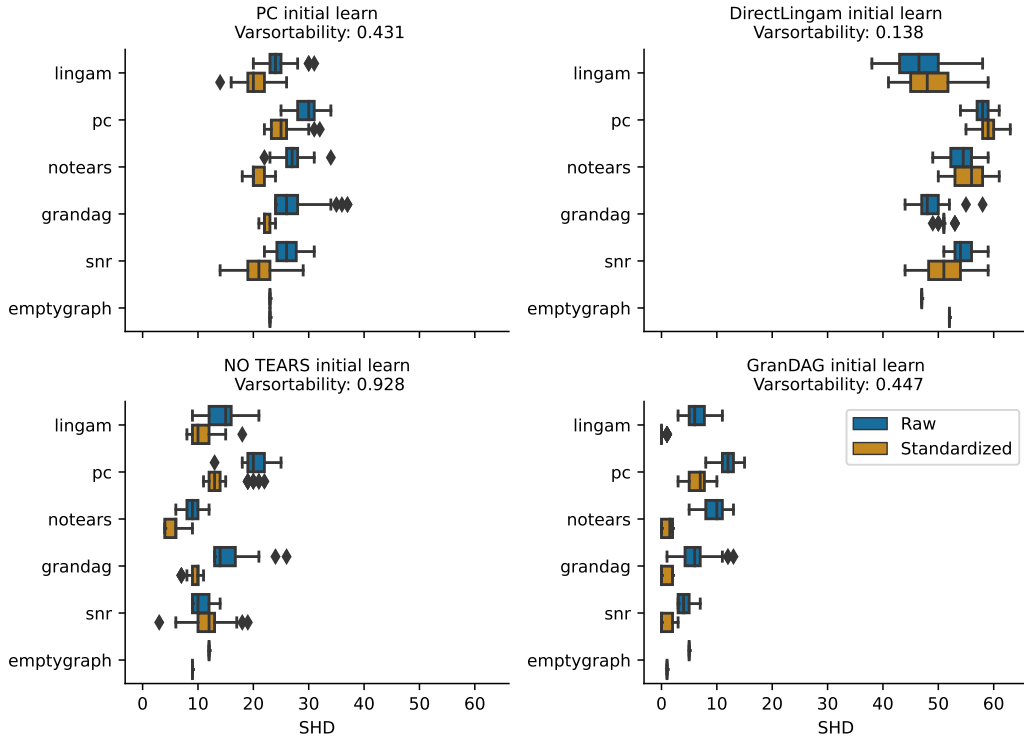


Figure 9: SHD for initial learning based on chosen causal discovery algorithms. Simulation run with 50 repetitions.

initial step. We demonstrate this on processes that take place in Station 3 consisting of 16 nodes. As not all methods considered are able to handle the inclusion of prior knowledge, we ignore existing process knowledge and learn from the data only.

Figures 9 and 10 report SHD and F_1 score between the ground truth DAG learned by the initial causal discovery procedure and results based on corresponding semisynthetic data.

Next to overall patterns left by the initial learning step, we present sensitivity results with respect to measurement scale. The real data obtained from the process control unit carry a wide range of different measurement scales. These scales should ideally be irrelevant with respect to causal relationships.

In a first step, we keep the raw data scale both for the initial learning and for the benchmark run based on the obtained ground truth. We report the average varsortability across simulation runs. In a second step, we standardize all data. We also report results for the empty graph to keep track of the number of edges inferred during the initial graph learning step. If the SHD of the empty graph changes under standardization then data scale has an effect on the initial ground truth.

DirectLiNGAM, NOTEARS, and GraN-DAG show a clear performance edge when the ground truth is originally obtained using the respective routine. This pattern is most clear in Figure 10. The PC algorithm does not seem to benefit too greatly which can to some degree be attributed to the random DAG completion. In contrast to the remaining methods, the PC algorithm is agnostic to measurement scale. DirectLiNGAM is in theory also scale agnostic, however scaling may influence the adjacency matrix estimation via adaptive lasso when predictors are not standardized. Regarding NOTEARS and GraN-DAG measurement units play a substantial role. NOTEARS obtains a ground truth with varsortability close to one on unstandardized data and recovers a very sparse DAG on standardized data. This suggests that NOTEARS essentially orders variables according to their variances when learned on raw data. GraN-DAG results are highly variable throughout all initial learning methods. The instability becomes particularly severe when applied to standardized data.

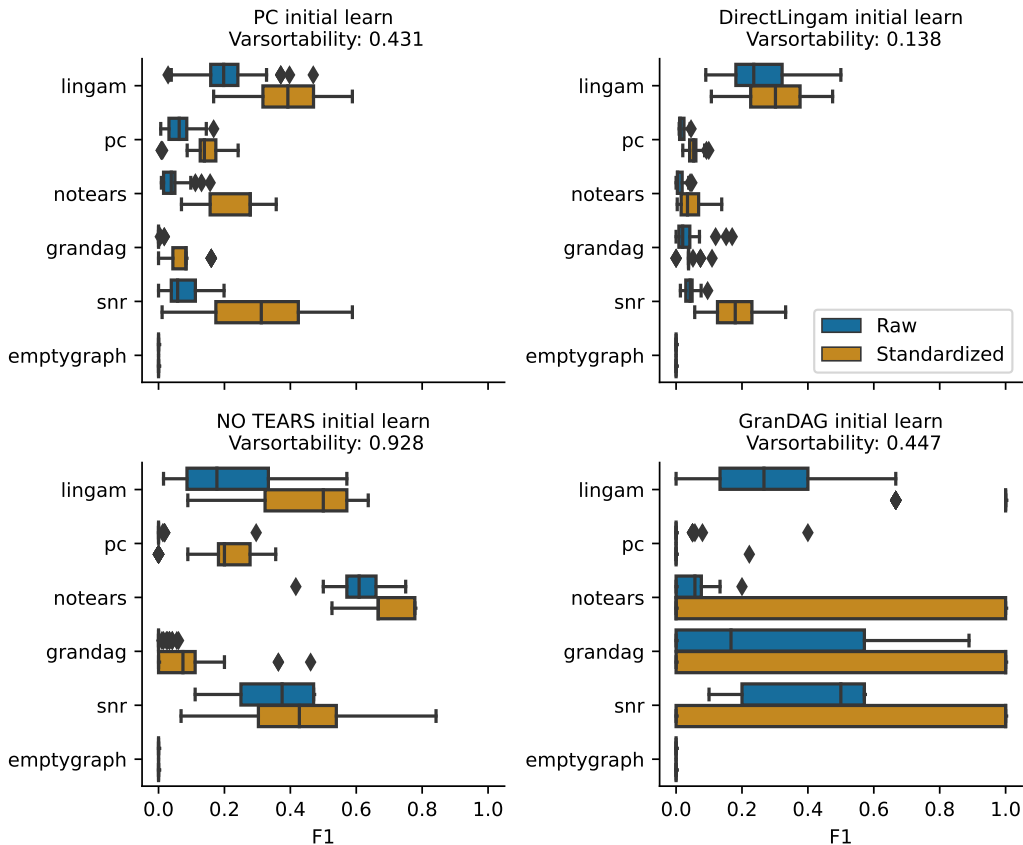


Figure 10: F_1 score for initial learning based on chosen causal discovery algorithms. Simulation run with 50 repetitions.

Overall, except for the PC algorithm there are clear traces left by initial learning algorithms applied to process cell structure learning discovery.

C Benchmarking

C.1 Algorithms and metrics

Algorithms The following well-known structure learning algorithms are employed in our work.

PC algorithm [16] (pc)

A constraint based algorithm that in a first step performs conditional independence tests in a resource efficient way returning a skeleton and in a second step orients as many edges as possible. We use the stable version of the algorithm proposed by [51]. Conditional independence tests are performed using Fisher z-transformed (partial) Pearson correlation coefficients. Since the PC algorithm outputs a completed partially directed acyclic graph (CPDAG), we choose in each run a random DAG that is a member of the MEC implied by the CPDAG.

DirectLiNGAM [17, 52] (lingam)

The direct method to learning the LiNGAM model [27] referred to in Section 2.2. First, the procedure detects source variables by employing entropy-based measures to find independence between the error variables. The *most independent* variable is placed first in the causal order and its effect removed from the other variables. As the ordering of the residuals resembles that of the variables themselves the algorithm continues to find the next variable in the ordering by finding the next *source*-residual.

Table 3: All benchmarks are run on a Linux machine with 32 GB Memory and 8 cores.

Result	Compute time
Full assembly line benchmark Fig 6 in the main text	16.90 hours
Station 1 benchmark Fig 11	1.07 hours
Station 2 benchmark Fig 12	4.39 hours
Station 3 benchmark Fig 13	2.22 hours
Station 4 benchmark Fig 14	3.54 hours
Station 5 benchmark Fig 15	2.33 hours

NOTEARS [18, 53] (`notears`)

A score-based method that recasts the discrete DAG constraint as a continuous equality constraint. This allows for the application of a wide range of techniques for non-convex programs. In NOTEARS a linear SEM is assumed and for each variable, a feed-forward neural network is trained that gets all other variables as input. The graph structure is then dynamically read-off from the networks during training by aggregating the weights of the input layer of each network. Acyclicity of the graph is enforced by training the networks simultaneously in an augmented Lagrangian schema such that the matrix exponential of the adjacency matrix has small trace.

GrAN-DAG [19] (`grandag`)

A score-based method and an extension of NOTEARS. In contrast to NOTEARS, the relation structure is read-off from the networks by aggregating all the weights till the output layer of the neural networks individually.

sortnregress [11] (`snr`)

A diagnostic tool to expose data scenarios with high varsortability. The procedure sorts variables by increasing marginal variance and then regresses each variable on their ancestors adding an ℓ -1 type penalty to induce sparsity.

Metrics The choice of evaluation metrics for assessing causal discovery outcomes matters [see 8]. We employ a selection of common structural performance metrics and note that in a full scale benchmark these should be extended to include a greater variety of evaluation measures.

Structural hamming distance (SHD):

The SHD counts how many edge insertions, deletions, and reversals are necessary to turn the estimated DAG into the ground truth DAG.

Precision, Recall and F_1 score:

Precision in the graphical context refers to the fraction of correctly identified edges among all edges inferred. Recall, sets these correctly identified edges in relation to all edges present in the ground truth. The F_1 score is the harmonic mean of Precision and Recall, i.e. $F_1 = 2 \frac{\text{Precision} \cdot \text{Recall}}{\text{Precision} + \text{Recall}}$.

C.2 Additional benchmarking results

Table 3 states compute time for each of the benchmark scenarios.

We present additional benchmarks for the remaining production stations. Each simulation run, we sample from the DRF regrown on the corresponding cell graphs. We find that results vary substantially across stations. Figure 11 reports results for the first station. DirectLiNGAM performs best while NOTEARS is not able to detect any edges. GrAN-DAG and PC Algorithm results are very unstable throughout all benchmarks. In Figure 12 station two benchmarks are depicted. In this case, NOTEARS performs best. Figure 13 reports station three benchmarks where DirectLiNGAM and NOTEARS demonstrate similar performance. In Figure 14 station four benchmarks suggest that NOTEARS outperforms DirectLiNGAM in terms of SHD and precision. In terms of recall and F1 score however, DirectLiNGAM performs best. On station five (Figure 15) DirectLiNGAM overall performs best.

C.3 Hyper and tuning parameters

Table 4 reports all hyperparameters and tuning parameters used in this work.

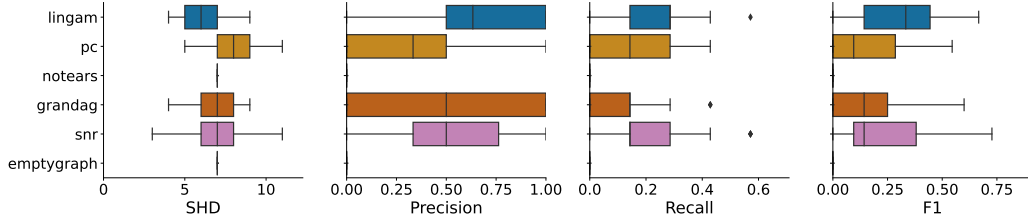


Figure 11: Chosen metrics for assessing causal discovery outcomes on Station 1 ($|V_1 \cup V_2| = 6$) using 100 simulation runs on a sample size of $n = 500$.

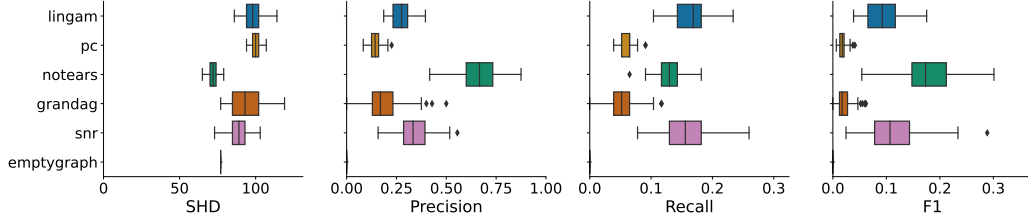


Figure 12: Chosen metrics for assessing causal discovery outcomes on Station 2 ($|V_3 \cup V_4| = 34$) using 100 simulation runs on a sample size of $n = 500$.

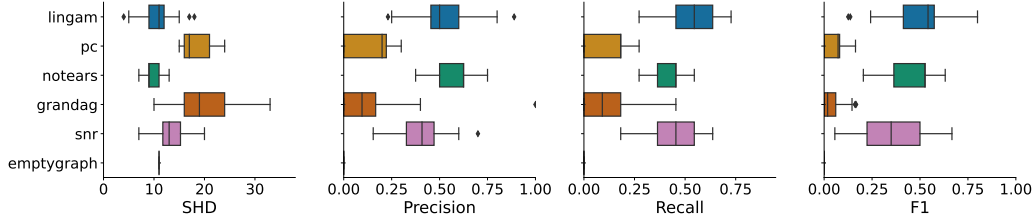


Figure 13: Chosen metrics for assessing causal discovery outcomes on Station 3 ($|V_5 \cup V_6| = 16$) using 100 simulation runs on a sample size of $n = 500$.

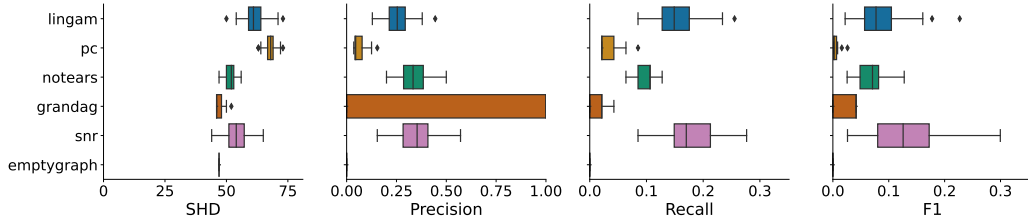


Figure 14: Chosen metrics for assessing causal discovery outcomes on Station 4 ($|V_7 \cup V_8| = 26$) using 100 simulation runs on a sample size of $n = 500$.

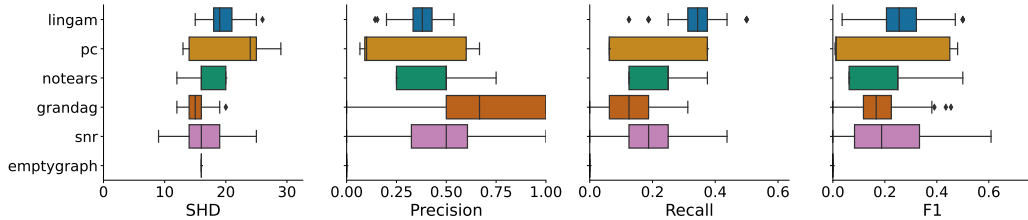


Figure 15: Chosen metrics for assessing causal discovery outcomes on Station 5 ($|V_9 \cup V_{10}| = 16$) using 100 simulation runs on a sample size of $n = 500$.

Table 4: Hyper and tuning parameter choices for routines employed in this work.

	Parameters
SpAM	<code>num_folds = 5</code> <code>cv_loss = MSE</code> <code>lambda_choice = lse</code> <code>num_bsplines = 6</code>
DRF	<code>min_node_size = 15</code> <code>num_trees = 2000</code> <code>splitting_rule = FourierMMD</code>
PC Algorithm	<code>indep_test : fisherz</code> <code>alpha = 0.05</code>
NOTEARS	<code>lambda_1 = 0.1</code> <code>loss_type = ℓ_2</code> <code>max_iter = 100</code> <code>h_tol = $1e - 8$</code> <code>rho_max = $1e + 16$</code> <code>w_threshold = 0.3</code>
GraN-DAG	<code>input_dim = V</code> <code>hidden_num = 2</code> <code>hidden_dim = 10</code> <code>batch_size = 64</code> <code>lr = 0.001</code> <code>iterations = 10000</code> <code>model_name = NonLinGaussANM</code> <code>nonlinear = leaky-relu</code> <code>optimizer = rmsprop</code> <code>h_threshold = $1e - 8$</code> <code>lambda_init = 0.0</code> <code>mu_init = 0.001</code> <code>omega_lambda = 0.0001</code> <code>omega_mu = 0.9</code> <code>stop_crit_win = 100</code> <code>edge_clamp_range = 0.0001</code>